IEEE Access
Multidisciplinary | Rapid Review | Open Access Journal

Received October 31, 2020, accepted November 18, 2020, date of publication November 25, 2020,
date of current version December 9, 2020.

Digital Object Identifier 10.1109/ACCESS.2020.3040420

An Ultra-Wideband Microwave Photonic Channelizer Based on Coherent Optical Frequency Combs and Image-Reject Down-Conversion

BO CHEN[1,2], YANGYU FAN[1], WUYING WANG[1], AND YONGSHENG GAO[1], (Member, IEEE)
[1]School of Electronics and Information, Northwestern Polytechnical University, Xi'an 710129, China
[2]School of Physics and Electronic Engineering, Xianyang Normal University, Xianyang 712000, China

Corresponding author: Yongsheng Gao (ysgao@nwpu.edu.cn)

This work was supported in part by the National Nature Science Foundation of China under Grant 61701412, in part by the National Postdoctoral Program for Innovative Talents under Grant BX201700197, in part by the Project funded by the China Postdoctoral Science Foundation under Grant 2017M623238, and in part by the sustainably supported Foundation by the National Key Laboratory of Science and Technology on Space Microwave under Grant HTKJ2019KL504011.

ABSTRACT Radio frequency (RF) channelization receiver is one of the most effective methods for processing ultra-wideband RF signals. In this paper, an ultra-wideband microwave photonic channelizer based on coherent optical frequency combs (OFCs) and image-reject down-converter is proposed and demonstrated. The OFCs used in the system are generated by two dual parallel Mach–Zehnder modulators (DPMZM), and the free spectrum range (FSR) is flexibly adjustable. The image-reject down-converter can not only effectively achieve image separation but also suppress the seven-order distortion and DC offset using balanced detection. A K- and Ka-band RF signal covering the frequency band from 25 to 30 GHz is sliced into 5 sub-channels with 1-GHz bandwidth, two-tone signals with frequencies of 27.5 and 27.51GHz are used to measure the spurious free dynamic range (SFDR) which is 116.8 dB·Hz $^{2/3}$, the image-rejection is over 66.4 dB, and the error vector magnitude (EVM) is 4.2%.

INDEX TERMS Microwave photonics, channelization, optical frequency comb (OFC), image rejection, balanced detection.

I. INTRODUCTION

As communication and radar detection technology develops, the bandwidth of the radio frequency (RF) signal is increasing rapidly. The broadband multi-service access and communication navigation identification in the civilian field [1], [2], and the frequency-agile radar and electronic warfare systems in the military field, have all put forward the need to manipulate wideband RF signals with the bandwidth of several GHz or even dozens of GHz in the future [3]. Therefore, RF receivers with large instantaneous bandwidth, high resolution, and large dynamic range are required to process multi-band signals arriving at the same time [4]–[7]. There are many effective approaches to realize the reception of ultra-wideband or multi-band signals, one of them is RF channelization receiver [8]. In an RF channelizer, the spectrum of the wideband RF signal is divided into different sub-channels through filter arrays, and then narrowband signals with different center frequencies are obtained in real time, which has a signal acquisition rate of almost 100% [9]. However, traditional channelized receiving technology is limited by the inherent electronic bottlenecks, such as large insertion loss, low dynamic range, serious electromagnetic interference and bulky size [10].

Fortunately, RF channelizers based on microwave photonic technology can solve the above drawbacks. In the last decade, several channelized receiving schemes based on microwave photonics have been reported. Among them, the channelized receiver implemented by spatial optical devices such as optical prisms usually have poor frequency resolution and large power loss [11], which is difficult to meet the development needs of modern electronic systems. As a special

The associate editor coordinating the review of this manuscript and approving it for publication was Di Zhang.

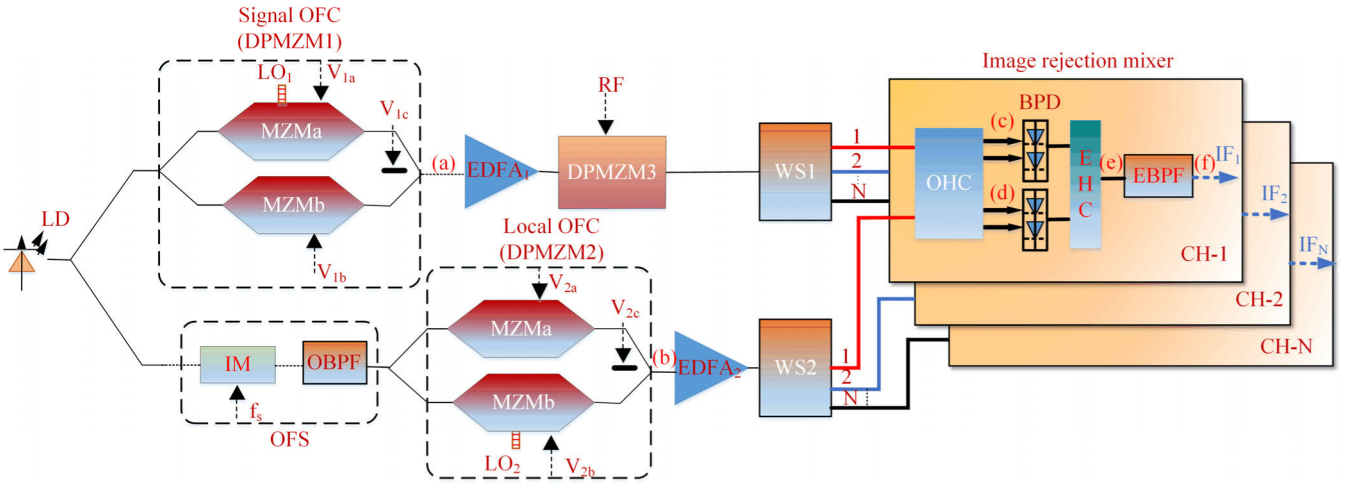

FIGURE 1. Schematic diagram of proposed microwave photonic channelizer. LD: laser diode; DPMZM: dual parallel Mach–Zehnder modulator; LO: local oscillator; EDFA: erbium-doped fiber amplifier; IM: intensity modulator; OBPF: optical bandpass filter; MZM: Mach-Zehnder modulator; PC: polarization controller; PBS: polarization beam splitter; OHC: optical hybrid coupler; BPD: balanced photodiode; EHC: electrical hybrid coupler; EBPF: electrical bandpass filter.

multi-wavelength coherent light source, optical frequency comb has the advantages of wide spectrum range and fixed repetition frequency [12], which is suitable for microwave photonic channelized receiver. In Ref. [9], a scheme based on dual optical combs with FP (Fabry-Perot) cavity filter is proposed, but the FP cavity filter cannot afford to supply the demanding Q factor and wavelength stability. In Ref. [13], a scheme based on a mode-locked laser and a dispersive fiber is proposed, but the generation scheme of dual optical combs is much complicated. Ref. [14] demonstrates a method which can suppress in-band interference greatly, but suffers the problems of second-order intermodulation distortion (IMD2) and DC offset. OFCs are widely used in many channelized receiving schemes, but it is difficult to generate ideal OFCs with a large number of comb lines, high flatness, and unwanted mode suppression ratio (UMSR) [15], [16], [18].

In this paper, a RF channelizer scheme is proposed, which consists of the generation of OFC and image-reject mixing. The OFC used in the scheme is generated by one DPMZM, and the FSR can be flexibly adjusted. A K- and Ka-band RF signal covering 25-30 GHz is sliced into 5 sub-channels with 1 GHz bandwidth. The system is mainly manipulated in the optical domain, which effectively overcomes the electronic bottleneck. The image-reject mixer can realize image separation of two signals in the same IF range [17]. Balanced detection is also applied in the scheme, which not only reduces the bandwidth and sampling rate requirements of the ADC, but also effectively suppresses the IMD2 and DC offset [19], [20], so that the SFDR of the proposed RF channelizer can reach 116.8 dB·Hz$^{2/3}$.

II. PRINCIPLE

As shown in Fig. 1, a continuous-wave (CW) light generated from a laser diode (LD) is launched into two branches by a 50:50 optical coupler and each one can be expressed as $E_{\text{in}}(t) = E_0 \exp(j2\pi f_c t)$, where E_0 is the amplitude and f_c is the frequency.

In the upper branch, only local oscillator (LO_1) signal is applied to drive MZMa and a push–pull configuration of the sub-MZMs is assumed. The LO_1 signal can be expressed as $V_{LO1} = V_0 \sin(\omega_{LO1} t)$, where V_0 is the amplitude and ω_{LO1} is the angular frequency.DPMZM1 have three DC bias voltages, which are denoted V_{1a}, V_{1b}, and V_{1c}, respectively. The output optical signal of the DPMZM1 can be expressed as:

$$E_{\text{DPMZM1}} = \frac{E_{in}(t)}{2}\left\{\cos\left[\frac{\pi V_0}{2V_\pi}\sin(2\pi f_{LO1}t) + \frac{\pi V_{1a}}{2V_\pi}\right] + \cos\left(\frac{\pi V_{1b}}{2V_\pi}\right)e^{j\frac{\pi V_{1c}}{V_\pi}}\right\} \quad (1)$$

In the equations, V_π is the half-wave voltage of the modulator. Optical carrier, first-order and second-order sidebands of the output optical signal can be written as (2-6) after Jacobi–Anger expansion.

$$E_0 = \frac{E_{in}(t)}{2}\left[\cos AJ_0(B) + \cos\left(\frac{\pi V_{1b}}{2V_\pi}\right)e^{j\frac{\pi V_{1c}}{V_\pi}}\right] \quad (2)$$

$$E_{+1} = \frac{E_{in}(t)}{2}\sin AJ_1(B)\,e^{j(2\pi f_{LO1}t+\frac{\pi}{2})} \quad (3)$$

$$E_{-1} = \frac{E_{in}(t)}{2}\sin AJ_1(B)\,e^{j(2\pi f_{LO1}t-\frac{\pi}{2})} \quad (4)$$

$$E_{+2} = \frac{E_{in}(t)}{2}\cos AJ_2(B)\,e^{j4\pi f_{LO1}t} \quad (5)$$

$$E_{-2} = \frac{E_{in}(t)}{2}\cos AJ_2(B)\,e^{-j4\pi f_{LO1}t} \quad (6)$$

where $A = \pi V_{1a}/2V_\pi$, $B = \pi V_0/2V_\pi$, and $J_n(\cdot)$ represent the nth-order Bessel function. The five lines of OFC are optical carrier, first-order and second-order sidebands, whose amplitude are closely related to the flatness of the five comb

lines. Where U is amplitude of the sidebands. It is obvious that five flat comb lines can be generated when (7-9) are satisfied.

$$\frac{E_{in}(t)}{2}\left[\cos AJ_0(B)+\cos\left(\frac{\pi V_{1b}}{2V_\pi}\right)e^{j\frac{\pi V_{1c}}{V_\pi}}\right]=-U \quad (7)$$

$$\frac{E_{in}(t)}{2}\left[\cos AJ_0(B)+\cos\left(\frac{\pi V_{1b}}{2V_\pi}\right)e^{j\frac{\pi V_{1c}}{V_\pi}}\right]=-U \quad (8)$$

After deformation, $V_{1a}V_{1b}$ and V_{1c} can be written as:

$$V_{1a}=\frac{2V_\pi}{\pi}\arctan\left[J_2(B)/J_1(B)\right] \quad (9)$$

$$V_{1c}=(2N+1)V_\pi,$$

$$\mathrm{V}_{1b}=\frac{2V_\pi}{\pi}\left\{\pm\arccos\left[\sin AJ_1(B)+\cos AJ_0(B)\right]\right\} \quad (10)$$

$$V_{1c}=2NV_\pi,$$

$$\mathrm{V}_{1b}=\frac{2V_\pi}{\pi}\left\{\pm\arccos\left[-\sin AJ_1(B)-\cos AJ_0(B)\right]\right\} \quad (11)$$

From (9)–(11), when the half-wave voltage of the MZM is 3.5 V and the modulation index (MI) is 0.83, the three DC bias voltages of DPMZM1 (V_{1a}, V_{1b} and V_{1c}) can be calculated as 3.15 V, −6.23 V, and 0 V, under the above condition, a five-line flat OFC can be generated.

If the values of V_{1a}, V_{1b}, and V_{1c} can be properly set in this OFC generation scheme, a seven-line flat OFC can also be generated. The output from DPMZM1 is expressed as the following equations:

$$E_{\mathrm{DPMZM1}}=\frac{E_{in}(t)}{2}\left\{\begin{array}{l}\left[\cos AJ_0(B)+\cos\left(\frac{\pi V_b}{2V_\pi}\right)e^{j\frac{\pi V_3}{V_\pi}}\right]\\+\sin AJ_1(B)e^{j(2\pi ft+\frac{\pi}{2})}+\sin AJ_1(B)\\\times e^{-j(2\pi ft+\frac{\pi}{2})}+\cos AJ_2(B)e^{j4\pi ft}\\+\cos AJ_2(B)e^{-j4\pi ft}+\sin AJ_3(B)e^{j(6\pi ft+\frac{\pi}{2})}\\+\sin AJ_3(B)e^{-j(6\pi ft+\frac{\pi}{2})}\end{array}\right\} \quad (12)$$

When the seven optical comb lines representing optical carrier, first-order, second-order sidebands and third-order sidebands have the same amplitude as (13) shows:

$$\frac{E_{in}(t)}{2}\sin AJ_1(B)=\frac{E_{in}(t)}{2}\cos AJ_2(B)=\frac{E_{in}(t)}{2}\sin AJ_3(B) \quad (13)$$

It can be easily calculated that $V_0=1.94\mathrm{V}_\pi$, $V_1=0.63\mathrm{V}_\pi$, $V_2=0.724\mathrm{V}_\pi$ and $V_3=\mathrm{V}_\pi$.

In this scheme, two five lines combs are used and denoted as signal OFC and local OFC, respectively. In the signal OFC, the frequency of each line can be written as:

$$f_{sig}(t)=\sum_{n=1}A_n\exp\left\{j2\pi\left[f_{sig}(1)+(\mathrm{n}-1)\delta_1\right]t\right\} \quad (14)$$

A_n represents the amplitude of the n^{th}-order comb line, $f_{sig}(1)$ represent the frequency of the first comb line and δ_1 represent the FSR of signal OFC. Being amplified by erbium-doped fiber amplifier (EDFA_1), the signal OFC is modulated by a wideband RF signal via a DPMZM3. DPMZM3 works under carrier suppressed single sideband (CS-SSB) condition, and β is the MI. The positive first-order sideband modulated by the RF signal can be written as:

$$f_{sig-\,\mathrm{mod}}(t)=\beta\sum_{n=1}A_n\exp\left\{j2\pi\left[f_{sig}(1)+(\mathrm{n}-1)\delta_1\right]\times t+f_{RF}(t)\right\} \quad (15)$$

In the lower branch, in order to make the local OFC and the signal OFC down-converted to the common IF, the frequency of optical carrier needs to be shifted via an optical frequency shifter (OFS). The OFS consists of intensity modulator (IM) and an optical bandpass filter (OBPF), in which the carrier is first modulated by a tone-signal with a frequency of f_s and then the positive first-order sideband is selected and launches into DPMZM2. The optical frequency comb generation principle in DPMZM2 is the same as that in DPMZM1. The frequency of each line in this local OFC can be expressed as:

$$f_{LO}(t)=\sum_{n=1}B_n\exp\left\{j2\pi\left[f_{LO}(1)+(\mathrm{n}-1)\delta_2\right]t\right\} \quad (16)$$

where B_n is the amplitude of the n^{th}-order comb line, $f_{LO}(1)$ is the frequency of the first comb line and δ_2 is the FSR of the local OFC, f^n_{center} is the center frequency of n^{th} channel and can be expressed as:

$$\begin{aligned}f^n_{center}&=\left[f_{LO}(1)+(n-1)\delta_2\right]-\left[f_{sig}(1)+(n-1)\delta_1\right]\\&=\left[f_{LO}(1)-f_{sig}(1)\right]+(n-1)(\delta_2-\delta_1)\end{aligned} \quad (17)$$

As can be seen clearly that f^n_{center} is closely related to both the order of the comb lines and the SFR of signal OFC and local OFC frequency, and the generation of OFC proposed in this scheme is flexibly adjustable.

In order to split the RF modulated OFC and the local OFC into different channels, the signals from the upper branch and the lower branch are sent to respective waveshapers, as is shown from the dashed lines in Fig. 2 (a) and (b).

Each channel contains a modulated RF sideband from the upper branch and a frequency-shifted LO comb line from the lower branch. These two signals are launched into an optical hybrid coupler (OHC) to achieve image-reject mixing. The optical signals output from the OHC can be written as:

$$E_1(t)=\left\{\begin{array}{l}\beta\sum_{n=1}A_n\exp\left\{j2\pi\left[f_{sig}(1)+(\mathrm{n}-1)\delta_1\right]t+f_{RF}(t)\right\}\cos\alpha\\+j\sum_{n=1}B_n\exp\left\{j2\pi\left[f_{LO}(1)+(\mathrm{n}-1)\delta_2\right]t\right\}\sin\alpha\exp(j\phi)\end{array}\right\} \quad (18)$$

$$E_2(t)=\left\{\begin{array}{l}\beta\sum_{n=1}A_n\exp\left\{j2\pi\left[f_{sig}(1)+(\mathrm{n}-1)\delta_1\right]t+f_{RF}(t)\right\}\sin\alpha\\-j\sum_{n=1}B_n\exp\left\{j2\pi\left[f_{LO}(1)+(\mathrm{n}-1)\delta_2\right]t\right\}\cos\alpha\exp(j\phi)\end{array}\right\} \quad (19)$$

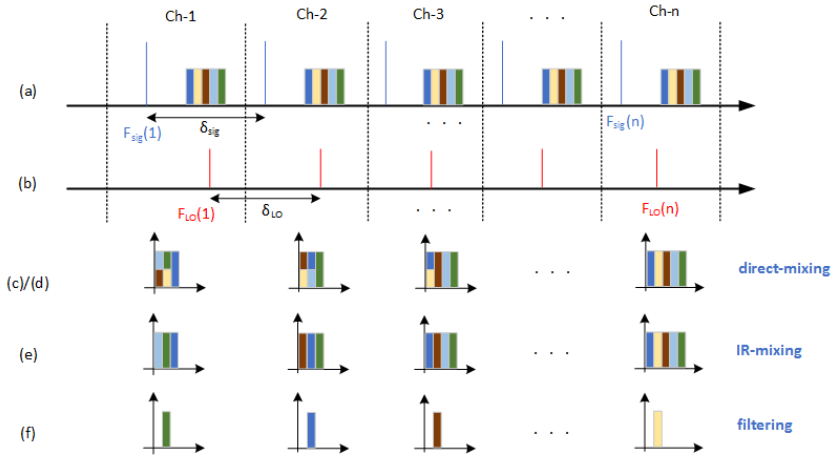

FIGURE 2. The schematic diagram of the proposed scheme.

After the balanced photodiode (BPD), a pair of in-phase and quadrature frequency down-converted signals can be obtained.

$$i_I(t) \propto A_n B_n \cos\left\{2\pi\left[f_{RF}(t) - f_{center}^n\right]\right\} t \quad (20)$$

$$i_Q(t) \propto A_n B_n \sin\left\{2\pi\left[f_{RF}(t) - f_{center}^n\right]\right\} t \quad (21)$$

Each channel contains a modulated RF sideband from the upper branch and a frequency-shifted LO comb line from the lower branch. These two signals are launched into an optical hybrid coupler (OHC) to achieve image-reject mixing. The optical signals output from the OHC can be written as:

$$E_1(t) = \begin{Bmatrix} \beta \sum_{n=1} A_n \exp\left\{j2\pi\left[f_{sig}(1)+(n-1)\delta_1\right]t + f_{RF}(t)\right\}\cos\alpha \\ +j\sum_{n=1} B_n \exp\left\{j2\pi\left[f_{LO}(1)+(n-1)\delta_2\right]t\right\}\sin\alpha\exp(j\phi) \end{Bmatrix} \quad (22)$$

$$E_2(t) = \begin{Bmatrix} \beta \sum_{n=1} A_n \exp\left\{j2\pi\left[f_{sig}(1)+(n-1)\delta_1\right]t + f_{RF}(t)\right\}\sin\alpha \\ -j\sum_{n=1} B_n \exp\left\{j2\pi\left[f_{LO}(1)+(n-1)\delta_2\right]t\right\}\cos\alpha\exp(j\phi) \end{Bmatrix} \quad (23)$$

After the balanced photodiode (BPD), a pair of in-phase and quadrature frequency down-converted signals can be obtained.

$$i_I(t) \propto A_n B_n \cos\left\{2\pi\left[f_{RF}(t) - f_{center}^n\right]\right\} t \quad (24)$$

$$i_Q(t) \propto A_n B_n \sin\left\{2\pi\left[f_{RF}(t) - f_{center}^n\right]\right\} t \quad (25)$$

As f_{center}^n is different in each channel, the modulated RF signals in different channels would be down-converted to the common IF band. Through Fig. 2(c–d), it can be easily found that the IF signal after down-conversion leads to a strong in-band image interference which can be hardly eliminated by electrical filters. In order to effectively suppress the image interference, an electrical hybrid coupler (EHC) is employed, which can easily separate the desired IF signal and the undesired image signal from the common IF band. The electrical spectra after image suppression are shown in Fig. 2(e). Finally, an electrical bandpass filter (EBPF) is used to filter out the desired corresponding IF signal in each sub-channel.

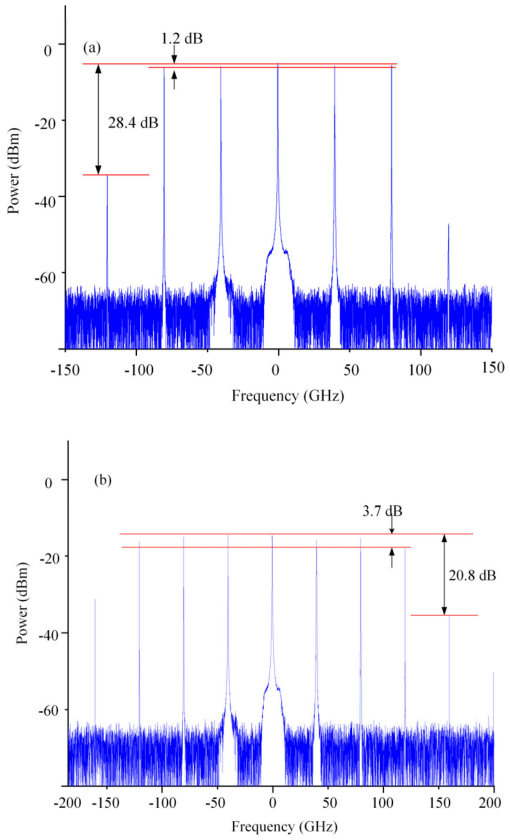

FIGURE 3. The optical frequency comb: (a) five lines; (b) seven lines.

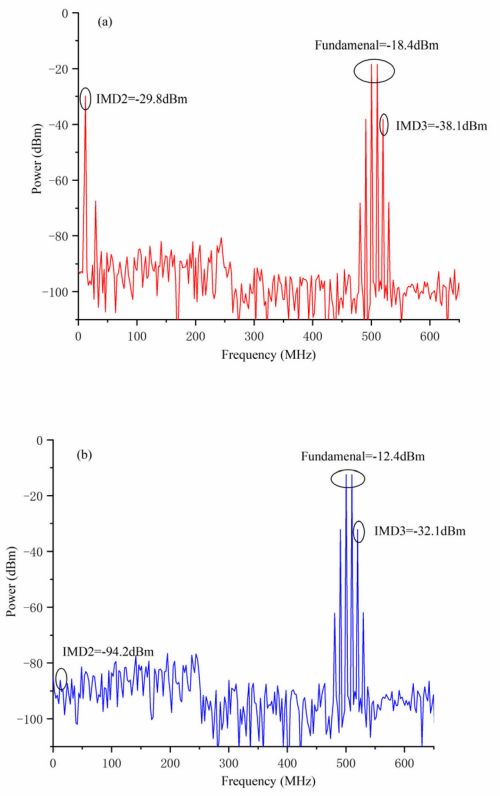

FIGURE 4. Down converted IF signals: (a) without balanced detection; (b) with balanced detection.

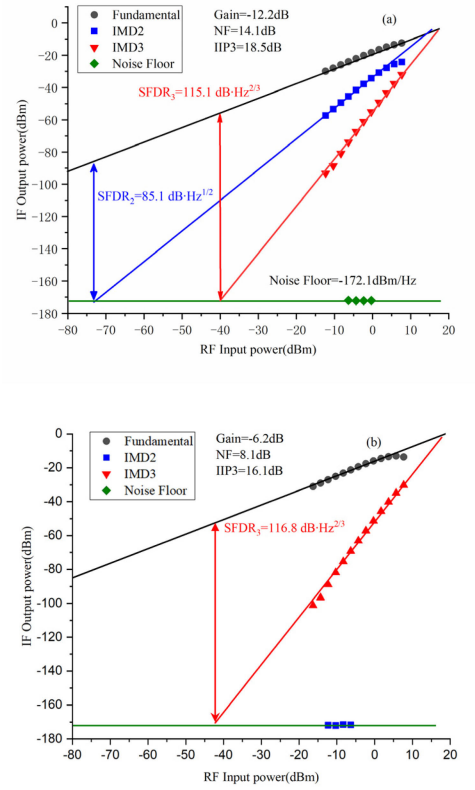

FIGURE 5. Measured powers of fundamental term, IMD2, IMD3 and noise floor in output IF signals as a function of RF input power. (a) without balanced detection; (b) with balanced detection. Two-tone RF frequencies: 27.5 and 27.51 GHz. LO frequency: 27 GHz. RF power: 0 dBm.

III. EXPERIMENT AND RESULTS

An experiment based on the configuration shown in Fig. 1is carried out. A continuous light wave with a frequency of 193.515 THz and average power of 16 dBm is generated by an LD (Conquer, KG-DFB-40-C36). The optical carrier is equally divided into two parts by optical couple (OC), In the upper branch, A DPMZM1 (Fujitsu FTM7961EX, V_π is 3.5V) is driven by a 40 GHz single-tone signal to generate signal OFC with the FSR of 40 GHz. The single-tone signal is generated by an analog signal generator (Agilent E8257D). The signal OFC is modulated by a wideband RF signal generated by a vector signal source (Agilent, E8267C) in DPMZM3 (Fujitsu FTM7961EX, V_π is 3.5 V).

In the lower branch, the optical carrier first uses an IM (Fujitsu FTM7937EZ, V_π is 3.5 V) and an OBPF (Yenista XTM-50) to achieve frequency shift and then sent to DPMZM2 (Fujitsu FTM7961EX, V_π is 3.5 V) to generate local OFC. The comb lines of the two OFCs are correspondingly separated by two parallel waveshapers (Finisar 16000S) and sent to the OHC (Kylia COH24) respectively. The output signals from OHC are sent to two BPDs (Finisar, BPDV2150R) to detect the electrical signals.

Fig. 3 shows the five lines and seven lines OFCs. It can be seen clearly that the higher-order sidebands are suppressed by more than 28.4 dB and 20.8 dB respectively, and the unflatness are 1.2 dB and 3.7 dB respectively. However, the increase in the number of optical combs will lead to the increase of modulation index and then the decrease in UMSR.

A two-tone signals testing is used to prove the optimization effect of balanced detection in the system. The frequencies of the two signals are 27.5 GHz and 27.51 GHz, with the powers of 0 dBm for down-conversion. The optical LO with the relative frequency of 27 GHz. The test result is shown in Fig. 4, the fundamental items (500 and 510 MHz) and IMD3 terms (490 and 520 MHz) both have 6-dB improvement after balanced detection. Meanwhile, the IMD2 is significantly suppressed by 64.4 dB, from −29.8 dBm to −94.2 dBm.

Both the SFDR with and without balanced detection are measured with the two-tone signals. Fig. 5(a) shows the result without balanced detection, and it can be easily calculated that the conversion gain is -12.2 dB and the noise figure (NF) is 14.1 dB. Although the SFDR3 reaches 115.1 dB · $Hz^{2/3}$, the IMD2 is the dominant distortion and drags the SFDR2 to only 85.1 dB·$Hz^{1/2}$, which determines the overall SFDR of the system. Fig. 5(b) shows the result with balanced detection, where the conversion gain is -6.2 dB. The fundamental and IMD3 terms have a 6 dB increase in amplitude after balanced detection, which agrees with the theoretical expectation. Since the simulation is under ideal conditions, the IMD2 is completely suppressed below the noise floor after balanced detection, so it is not drawn in Fig. 5(b).

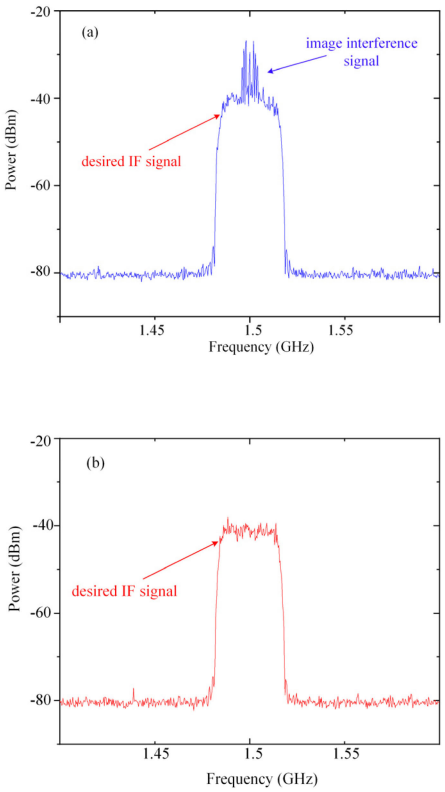

FIGURE 6. Image rejection test: (a) without image rejection; (c) with image rejection.

Since the proposed scheme is to achieve the common IF reception of ultra-wideband signals, the RF signals in different channels will be image interferences to each other after being down-converted to IF domain. The EHC after I/Q down-conversion can effectively achieve image rejection [21], [22]. Due to the lack of an ultra-wideband RF signal source, the 25-30 GHz wideband signal cannot be generated. Therefore, a wideband signal with a center frequency of 25.5GHz (in channel 1) and a bandwidth of 30 MHz is used as the desired signal, another wideband signal with a center frequency of 28.5 (in channel 4) and a bandwidth of 10 MHz is used as the image interference signal.

The results of image rejection test are shown in Fig. (6). Fig. 6(a) shows that the signals after down-conversion are in the same IF range (1–2 GHz) and the IF signals in channel 1 and channel 4 are image interferences for each other. Fig. 6(b) shows that the IF signal in channel 4 is well suppressed as an image signal, and the suppression effect is deteriorated because of the amplitude and phase imbalance in the EHC. Unlike image interferences, the crosstalk is mainly caused by the residual optical carrier and sidebands. In order to distinguish the influence of other sub-channels on channel 1, we used five single-tone signals with different center frequencies to down-convert to the same IF range from 1.5 GHz to 1.55 GHz and the result is shown in Fig. 7. We can clearly find the channel isolations are all over 22 dB, and 24.1 dB is the image rejection of channel 1 to channel 4.

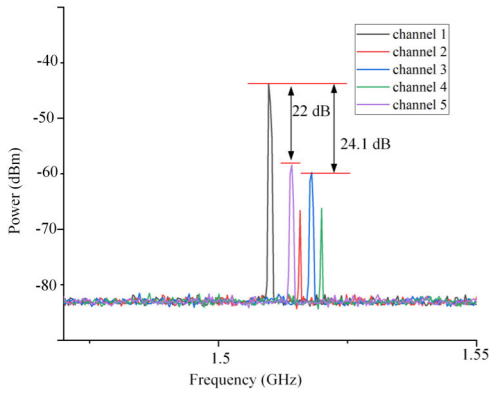

FIGURE 7. Measured channel crosstalk influence of other sub-channels on channel 1.

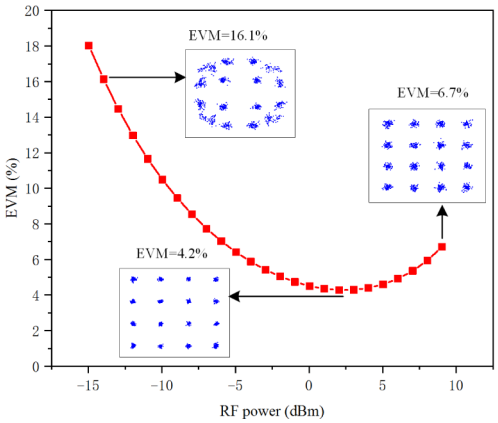

FIGURE 8. Measured EVM and constellation diagram.

Fig. 8 shows the changes in the EVM curves and constellation diagrams with the increase of input power of the RF signal. It is clear that when the RF power ranges from −15 dBm to 10 dBm, the EVM decreases rapidly at first until reaching the bottom at about 4.2%, which is the optimum point of the input RF power. After the optimum point, the IMD3 increases significantly, which deteriorates the constellation diagrams and thus the EVM begins to increase. With the RF power from −10 dBm to 7 dBm, the EVM is below 10%, indicating a large dynamic range of the system.

IV. CONCLUSION

A wideband microwave photonic channelization receiver based on dual OFC is proposed and demonstrated by experiment in this paper. The OFC generated by a DPMZM has high flatness and the FSR is flexibly adjustable. An ultra-wideband RF signal can be sliced into 5 sub-channels with 1 GHz bandwidth. It is worth mentioning that the balanced detected image-reject mixer not only suppresses the image interference, but also suppresses the IMD2 and DC offset, which can effectively improve the dynamic range of the system to 116.8 dB $Hz^{2/3}$. The proposed photonic microwave channelizer may have great application prospect in the future electronic warfare, radar system and satellite communication fields.

REFERENCES

[1] J. Capmany and D. Novak, "Microwave photonics combines two worlds," *Nature Photon.*, vol. 1, no. 6, pp. 319–330, Jun. 2007.

[2] C. H. Cox, E. I. Ackerman, G. E. Betts, and J. L. Prince, "Limits on the performance of RF-over-fiber links and their impact on device design," *IEEE Trans. Microw. Theory Techn.*, vol. 54, no. 2, pp. 906–920, Feb. 2006.

[3] V. R. Pagán and T. E. Murphy, "Electro-optic millimeter-wave harmonic downconversion and vector demodulation using cascaded phase modulation and optical filtering," *Opt. Lett.*, vol. 40, no. 11, p. 2481, Jun. 2015.

[4] R. Emrick, P. Cruz, N. B. Carvalho, S. Gao, R. Quay, and P. Waltereit, "The Sky's the limit: Key technology and market trends in satellite communications," *IEEE Microw. Mag.*, vol. 15, no. 2, pp. 65–78, Mar. 2014.

[5] A. D. Panagopoulos, P.-D.-M. Arapoglou, and P. G. Cottis, "Satellite communications at KU, KA, and v bands: Propagation impairments and mitigation techniques," *IEEE Commun. Surveys Tuts.*, vol. 6, no. 3, pp. 2–14, 3rd Quart., 2004.

[6] R. W. Ridgway, C. L. Dohrman, and J. A. Conway, "Microwave photonics programs at DAPRA," *J. Lightw. Technol.*, vol. 32, no. 20, pp. 3248–3249, Jan. 18, 2014.

[7] T. Kuri, H. Toda, and K. Kitayama, "Dense wavelength-division multiplexing millimeter-wave-band radio-on-fiber signal transmission with photonic downconversion," *J. Lightw. Technol.*, vol. 21, no. 6, pp. 1510–1517, Jun. 2003.

[8] D. Lam, A. M. Fard, B. Buckley, and B. Jalali, "Digital broadband linearization of optical links," *Opt. Lett.*, vol. 38, no. 4, p. 446, Feb. 2013.

[9] X. Xie, Y. Dai, K. Xu, J. Niu, R. Wang, L. Yan, and J. Lin, "Broadband photonic RF channelization based on coherent optical frequency combs and I/Q demodulators," *IEEE Photon. J.*, vol. 4, no. 4, pp. 1196–1202, Aug. 2012.

[10] L. X. Wang, N. H. Zhu, W. Li, H. Wang, J. Y. Zheng, and J. G. Liu, "Polarization division multiplexed photonic radio-frequency channelizer using an optical comb," *Opt. Commun.*, vol. 286, pp. 282–287, Jan. 2013.

[11] Q. Wang, L. Huo, Y. Xing, and B. Zhou, "Ultra-flat optical frequency comb generator using a single-driven dual-parallel Mach–Zehnder modulator," *Opt. Lett.*, vol. 39, no. 10, p. 3050, May 2014.

[12] J. Wang, M. Chen, Y. Liang, H. Chen, S. Yang, and S. Xie, "Broadband RF front-end using microwave photonics filter," *Opt. Exp.*, vol. 23, no. 2, p. 839, Jan. 2015.

[13] W. Hao, Y. Dai, F. Yin, Y. Zhou, J. Li, J. Dai, W. Li, and K. Xu, "Chirped-pulse-based broadband RF channelization implemented by a mode-locked laser and dispersion," *Opt. Lett.*, vol. 42, no. 24, p. 5234, Dec. 2017.

[14] Z. Tang and S. Pan, "Image-reject mixer with large suppression of mixing spurs based on a photonic microwave phase shifter," *J. Lightw. Technol.*, vol. 34, no. 20, pp. 4729–4735, Oct. 15, 2016.

[15] X. Yang, K. Xu, J. Yin, Y. Dai, F. Yin, J. Li, H. Lu, T. Liu, and Y. Ji, "Optical frequency comb based multi-band microwave frequency conversion for satellite applications," *Opt. Exp.*, vol. 22, no. 1, p. 869, Jan. 2014.

[16] W. Jiang, S. Zhao, Q. Tan, D. Liang, X. Li, and Y. Gao, "Wideband photonic microwave channelization and image-reject down-conversion," *Opt. Commun.*, vol. 445, pp. 41–49, Aug. 2019.

[17] Z. Tang and S. Pan, "A reconfigurable photonic microwave mixer using a 90° optical hybrid," *IEEE Trans. Microw. Theory Techn.*, vol. 64, no. 9, pp. 3017–3025, Sep. 2016.

[18] Z. Tang, D. Zhu, and S. Pan, "Coherent optical RF channelizer with large instantaneous bandwidth and large in-band interference suppression," *J. Lightw. Technol.*, vol. 36, no. 19, pp. 4219–4226, Oct. 2018.

[19] Y. Gao, A. Wen, W. Zhang, W. Jiang, J. Ge, and Y. Fan, "Ultra-wideband photonic microwave I/Q mixer for zero-IF receiver," *IEEE Trans. Microw. Theory Techn.*, vol. 65, no. 11, pp. 4513–4525, Nov. 2017.

[20] Y. Gao, A. Wen, W. Jiang, Y. Fan, and Y. He, "All-optical and broadband microwave fundamental/sub-harmonic I/Q down-converters," *Opt. Exp.*, vol. 26, no. 6, p. 7336, Mar. 2018.

[21] S. T. Lipkowitz, T. U. Horton, and T. E. Murphy, "Wideband microwave electro-optic image rejection mixer," *Opt. Lett.*, vol. 44, no. 19, p. 4710, Oct. 2019.

[22] B. M. Haas and J. D. McKinney, "A band-folding microwave photonic link with inter-band image rejection," *IEEE Photon. Technol. Lett.*, vol. 32, no. 1, pp. 39–42, Jan. 1, 2020.

BO CHEN received the B.S. degree in optical engineering from Xi'an Technological University, Xi'an, China, in 2010. He is currently pursuing the Ph.D. degree in microwave photonics and optical channelization with the School of Electronics and Information, Northwestern Polytechnical University, Xi'an.

YANGYU FAN received the M.S. degree in electromechanical engineering from the Shaanxi University of Science and Technology, Xi'an, China, in 1992, and the Ph.D. degree in acoustics signal processing from Northwestern Polytechnical University, Xi'an, in 1999.

He is currently a Professor with the School of Electronics and Information, Northwestern Polytechnical University. His research interests include optical communications, image processing, pattern recognition, and virtual reality.

WUYING WANG received the B.E. degree from Guangxi University, Nanning, China, in 2005, and the M.S. degree from the Guilin University of Electronic Technology, Guilin, China, in 2009. He is currently pursuing the Ph.D. degree with the School of Electronics and Information, Northwestern Polytechnical University. His current research interests include radio-over-fiber techniques and microwave photonics radar signal generation and processing.

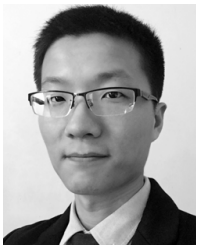

YONGSHENG GAO (Member, IEEE) received the B.E., M.S., and Ph.D. degrees from the School of Telecommunications Engineering, Xidian University, China, in 2011, 2014, and 2016, respectively.

He is currently an Associate Professor with the School of Electronics and Information, Northwestern Polytechnical University. He has published over 40 research articles in various journals and conference proceedings. His current research interests include microwave photonics and radio-over-fiber techniques.